Mechanical and Thermal Spreading of Antimony Oxides on the TiO_2 Surface: Dispersion and Properties of Surface Antimony Oxide Species†

Bernhard Pillep‡ and Peter Behrens*,§

Institut für Anorganische Chemie, Ludwig-Maximilians Universität München, Meiserstrasse 1, 80333 München, Germany

Uwe-Anton Schubert,|| Jörg Spengler,⊥ and Helmut Knözinger*

Institut für Physikalische Chemie, Ludwig-Maximilians Universität München,Butenandtstr. 5−13, Haus E, 81377 München, Germany

Received: May 3, 1999; In Final Form: July 15, 1999

Mixed metal oxides are important industrial catalysts for the selective oxidation and ammoxidation of aromatics and alkenes and often contain Sb oxides as a component. For the preparation of a catalytically relevant system on the basis of monolayer-type catalysts, an alternative route as compared to the conventional impregnation was chosen by milling the dry compounds in a planetary mill. To get a closer insight into the spreading and oxidation properties of antimony oxide on titania, only the binary oxidic compounds Sb oxide and TiO_2 as support were investigated in the present study. Photoelectron spectroscopy (XPS) investigations for surface analysis and X-ray absorption spectroscopy (XANES) for bulk phase analysis were applied. The various Sb oxides (Sb_2O_3, Sb_2O_4, and Sb_2O_5) show totally different spreading behavior. Only with the Sb(III) oxide on titania a significant increase of dispersion was detectable by means of XPS and temperature programmed reduction (TPR). The temperature of oxidation of the supported Sb(III) oxide in air was 100 °C lower as compared to the bulk phase oxidation. The final formula after oxidation of Sb(III) oxide can be calculated from XANES results as Sb_6O_{13} and does not end up at a stoichiometry of Sb_2O_4.

Introduction

The catalytic oxygen and nitrogen functionalization of alkenes, alkanes, and aromatics is of high industrial importance, because of the economic value of the products and the abundant availability of feedstocks out of petroleum.[1] One example is the synthesis of phthalic anhydride (PA) by oxidation of *o*-xylene with a worldwide capacity of 3.2×10^6 t per year in 1991. PA is used for the synthesis of softeners, polyester resins, dyes based on phthalocyanine, and fine chemicals.[2]

Besides vanadium oxide, Sb oxide is an essential component of industrial catalysts for the selective oxidation of substituted aromatics[3] and for the ammoxidation of paraffins to the corresponding unsaturated acids and nitriles.[4] Also, the oxidation of alkanes can be realized by mixed V/Sb oxide catalysts.[5] In the case of V-oxide-based catalysts, the published literature describes a variety of detailed models of the local coordination of the V species[1,6] and proposed reaction mechanisms.[7,8] The latter are often based on the Mars−van Krevelen mechanism.[9] On the other hand, there is little information available about the chemical and structural characterization of Sb oxide compounds supported on titania, in so-called monolayer type catalysts. Therefore, the results presented here are confined to the spreading behavior of pure Sb oxides on titania.

The preparation of the supported Sb oxide was not carried out via impregnation from solution, although this is the most common route to yield monolayer-type catalysts,[10] but rather via dry mechanical activation of the solids by ball milling. During this mechanical activation, accelerations in the range of 40 to 60 g ($g = 9.81\ ms^{-2}$) were measured, so that solid-state reactions are possible under these conditions.[11] This mechanochemical treatment of the powder materials was previously used in the field of metallurgy to overcome many limitations of conventional alloying.[12] It is also applicable in the field of catalyst generation.[13] Haber et al.[13] have shown for V_2O_5 that mechanical treatment of catalytically active oxides is a possible route to modify morphology and texture of unsupported catalysts and also for titania-supported active species. Milling also increases the activity and selectivity of V_2O_5/TiO_2 in the case of catalytic partial oxidation of *o*-xylene to phthalic anhydride.[13,14]

The aim of the present investigation was the elucidation of the spreading behavior of antimony oxides on anatase and also of the oxidation states of antimony in the prepared catalyst precursors. In addition to temperature-programmed reduction (TPR) and X-ray photoelectron spectroscopy (XPS), X-ray absorption fine structure (XAFS) measurements were performed. XAFS spectroscopy is well suited for these purposes. First, the energy position of the absorption edge is known to be a function of the effective charge on the absorbing atoms[15] and the intensities of peaks occurring at the edge as a result of dipole-allowed electronic transitions depend on the electron population

† Dedicated to Prof. Dr. M. Baerns on the occasion of his 65th birthday.

* To whom correspondence should be addressed.

‡ Present address: Patent- und Rechtsanwaltskanzlei Kador und Partner, Corneliusstrasse 15, 80469 München, Germany.

§ Present address: Institut für Anorganische Chemie, Universität Hannover, Callinstrasse 9, 30167 Hannover, Germany.

|| Present address: Carl Zeiss Lithos GmbH, Carl-Zeiss-Strasse, 73447 Oberkochen, Germany.

⊥ Present address: Consortium für die elektrochemische Industrie GmbH, Zielstattstrasse 20, 81379 München.

10.1021/jp991441b CCC: $18.00
Published on Web 10/07/1999

of the corresponding final states. These features of XAFS spectra allow the determination of oxidation states and also of the relative amounts of Sb(III) and Sb(V) in the investigated samples. Second, spectral structures in the energy region near the absorption edge, known as X-ray absorption near edge structure (XANES), are very sensitive to changes in the medium range (<7 Å) order around the absorbing atoms.[15,16] Third, the analysis of the extended X-ray absorption fine structure (EXAFS) yields an element-selective radial distribution function around the absorbing atoms and hence indicates changes in the first or higher coordination shells of these atoms. Thus, changes of the environment of the Sb atoms caused by the milling and calcination processes can also be detected by XAFS spectroscopy.

The XANES measurements were performed at the Sb L_1 edge to obtain high-resolution spectra. In addition to the spectra from the samples investigated, spectra of a series of reference compounds were also measured. EXAFS spectra were recorded at the Sb *K* edge because the positions of the Sb *L* edges are too closely spaced on the energy scale to yield reasonable EXAFS signals at the Sb L_2 and L_3 edges and Sb L_1 *e*dge EXAFS of the titania-supported samples cannot be obtained because of the onset of the Ti *K* edge at 4.97 keV, closely above the Sb L_1 edge.

Experimental Section

Sample Preparation. For catalyst preparation, commercial Sb_2O_3, Sb_2O_4, Sb_2O_5 (Fluka, p.a.) were used. In the case of Sb_2O_5 the oxidation state was not proven by the producer and it is shown in this work that it is not a pure Sb(V) compound. This commercial product is therefore denoted "Sb_2O_5" throughout this paper. The TiO_2 (TiO_2 suspension, dried and calcined at 873 K for 10 h) was pure anatase with a specific surface area (SA) of 45 m^2/g.

The mechanical treatment was performed in a planetary mill in air with either the dry oxidic compounds or with addition of 10 wt % H_2O. For that purpose, the oxides were mixed carefully in a mortar and then milled (145 rpm) in a vessel (250 mL) with six agate balls (1.5 cm in diameter). The time of milling was chosen between 1 and 20 h. After 1, 2, 3, 5, and 10 h the milling procedure was interrupted for sampling and loosening up of compressed powder pressed against the wall of the vessel. Since the effect of milling depends drastically on the amount of starting material, all milling preparations were carried out with an initial loading of 50 g of the mixed oxides.

The theoretical monolayer capacity of Sb_2O_3 was estimated by the formula of Roozeboom et al.[17] This leads to a monolayer capacity of 10 wt % of Sb_2O_3 on TiO_2 (the notation 1 ML Sb_2O_3/TiO_2 is used throughout this paper for this sample composition and is meant to characterize only the loading but is not supposed to infer the formation of a true monolayer).

For comparison purposes, one sample was prepared by impregnation from an aqueous Sb(III)−acetate solution followed by drying at 383 K and calcination at 673 K for 5 h.

The specific surface areas (SA) were measured after evacuation to 5.0×10^{-4} mbar and heating to 373 K for 2 h by the BET method on a Sorptomatic 1800 (Carlo Erba). For X-ray diffraction analysis a Siemens−Guinier diffractometer with CuK_α radiation was used.

The TPR experiments were performed in a flow apparatus with 5% H_2 (2.006×10^{-6} mol/mL) in N_2, at a flow rate of 11.4 mL/min. The heating rate was 10 K/min and the H_2 consumption was measured by a thermal conductivity detector (TCD). The amount of supported Sb_2O_3 sample for the TPR experiment was chosen such that the Sb oxide content was about 10 mg.

XPS measurements were carried out on a modified Vacuum Science Workshop (VSW ESCA 100) stainless steel UHV system. The base pressure in the analyzer chamber was in the range of 2×10^{-10} hPa, measured with 10 mA emission of a Bayard−Alpert ionization gauge. During outgassing of the powder samples under X-ray radiation, the pressure in the analyzer chamber increased to a maximum of 5×10^{-8} hPa. The temperature of the samples rose during XPS measurements to ca. 330 K (measured by a Chromel/Alumel thermocouple). The system was equipped with a twin anode X-ray source with MgK_α and AlK_α radiation for XPS/AES. The hemispherical analyzer (VSW HA 100) was operated in the fixed analyzer transmission (FAT) mode at a pass energy of 22 eV. This guarantees an energy independent resolution of 0.6 eV over the entire range of detected kinetic energies of the photoelectrons. A channeltron was used as detector. The absolute energy resolution of the XP spectrometer was determined by the line width of the $Au4f_{7/2}$ signal. For a sputtered and annealed gold foil we found a full width at half maximum (fwhm) of 1.65 eV. The signal can be fitted with a Gaussian line shape and has a base width of nearly twice the width at half maximum.

The titania supported antimony oxide samples were pressed into a sample holder and transferred into the analyzer chamber via a fast entry and a prechamber (pumped by an oil diffusion pump 200 L/min) at a pressure below 2.0×10^{-8} hPa. The spectra accumulation and subsequent computer-aided treatment were carried out using the commercial program ECRUN (version 4.0, 1989 VSW). The emissions corresponding to C1s, $Sb3d_{3/2}$, Ti2p, and O1s were analyzed. For determination of signal intensities, the background was subtracted with a linear or integral algorithm, depending on the shape of the background. Charging effects and the work function of the samples were determined by referencing the corresponding signal to the C1s line of graphitic carbon at 284.4 eV or to the $Ti2p_{3/2}$ signal of TiO_2 at 258.5 eV.[18]

For the X-ray absorption measurements, carefully ground powders of the samples were pressed into polyethylene pellets (spectroscopic grade polyethylene, Merck 107422). The amount of sample was adjusted to give edge jumps $\Delta\mu d$ from 0.3 to 0.8.

Sb *L* edge and Sb *K* edge XAFS spectra were recorded at HASYLAB/DESY in Hamburg (Germany). The storage ring DORIS III was operated at 4.432 GeV with an injection current of 100 mA. All spectra were collected at room temperature in the transmission mode by monitoring the X-ray intensities with ionization chambers. Sb *L* edge spectra were measured at beamline E4, which is equipped with a focusing Ni-coated mirror and a Si (111) double-crystal monochromator. The edge region was scanned with a step width of 0.2 eV, well below the estimated experimental resolution of 0.8 eV. For the energy calibration, the Ca *K* edge of a $CaWO_4$ sample was recorded simultaneously with each sample. Sb *K* edge spectra were recorded at beamline X1.1. The spectrometer is equipped with a Si (311) double-crystal monochromator. The signal of a Sb foil was simultaneously recorded for energy calibration.

At both experiments, detuning of the monochromator to 50% of the maximum intensity served to reduce contributions of higher harmonics to the X-ray beam. At beamline E4, the reflectivity cutoff of the Ni mirror at about 7 keV further improved this reduction.

The spectra were processed using the program WinXAS.[19] For the energy calibration of the Sb *L* edge spectra, the first

TABLE 1: N_2−BET Surface Areas of the Pure Dry Milled TiO_2 and Sb_2O_3 Depending on the Duration of Milling

milling duration (h)	N_2−BET surface area (m^2/g)	
	TiO_2	Sb_2O_3
0	45	1.5
1	48	1.5
2	50	15
3	51	18
5	51	19
10	52	20
20	53	18

inflection point of the Ca *K* edge was set to a value of 4.0491 keV. This corresponds to a value of 4.966 keV for the first inflection point at the Ti *K* edge of a Ti foil. The background was modeled using Victoreen-type functions and was subtracted from the curves. The edge jump $\Delta\mu d$ was normalized to an absorption value of 1. The positions of the white lines (WLs) at the Sb L_1 edge were determined from the first derivatives of the spectra.

The Sb *K* edge EXAFS spectra were energy calibrated by setting the first inflection point at the Sb *K* edge of Sb metal to 30.491 keV. Background correction and normalization were performed as for the Sb *L* edge spectra. After conversion into *k*-space, the EXAFS signals were extracted by cubic spline fits, weighted with k^3, and Fourier transformed in the range from 2.5 to 16 $Å^{-1}$.

Results and Discussion

Pure Unsupported Oxides. Milling of pure Sb_2O_3 leads to a significant increase of the BET surface area after 20 h from 1.5 to 18 m^2/g (see Table 1). In the case of pure TiO_2 the surface increases only slightly from 45 m^2/g for the untreated sample to 53 m^2/g after 20 h milling under the conditions described above. From scanning electron (SEM) and transmission electron (TEM) micrographs of the pure TiO_2 in the anatase modification (not shown) it can be concluded that the spherical shape of the agglomerates of primary particles remains unaffected by the mechanical treatment, also after 20 h milling. In SEM micrographs the particles of untreated samples and after 20 h milling were largely identical in size and structure when a particle size fraction between 100 and 200 nm was used. No indication for rutilization of the TiO_2 was seen. The mean size of the primary particles was about 40 to 60 nm. The agglomerates also having spherical shape had a mean size of 15 to 20 μm. The increase of the specific surface area after 20 h milling might be a consequence of breaking up some agglomerates, but the mean shape of the particles is unaffected by the mechanical treatment.

The increase of the Sb_2O_3 surface area is accompanied by a partial change of the crystallographic modification of the Sb_2O_3 from senarmontite to valentinite, as seen in XRD.

SEM micrographs of pure Sb_2O_3 samples clearly show morphological and structural effects of the milling on the primary particles of Sb oxide (not shown). Micrographs of the untreated and the 1, 5, and 20 h milled Sb_2O_3 samples were compared. During milling the spherical hollow spaces containing primary particles change into a more flat irregular sheetlike morphology.

From the XP peak position of the $Sb3d_{3/2}$ emission at 239.4 eV and the O1s emission at 530.2 eV (literature reference for Sb_2O_3: E_b = 239.4 eV of $Sb3d_{3/2}$ and E_b = 529.9 eV of O1s),[20] there was no evidence for oxidation of the pure Sb_2O_3 induced by milling even after 20 h. Also, the $O1s/Sb3d_{3/2}$ intensity ratio of 1.4 and the fwhm of the $Sb3d_{3/2}$ signal did not change during milling.

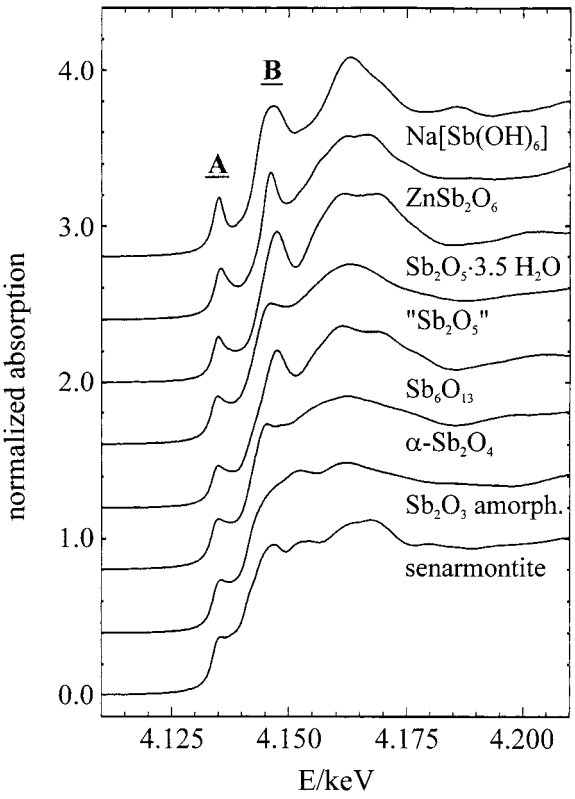

Figure 1. SbL_3 edge XANES spectra of selected oxidic antimony compounds. The spectra are arranged from bottom to top by increasing average oxidation state of the Sb atoms.

TABLE 2: XPS Binding Energies (eV) of the Pure TiO_2 and FWHM (eV) Depending on the Duration of Milling

milling duration (h)	$Ti2p_{3/2}$	fwhm	O1s	fwhm	$O1s/Ti2p_{3/2}$ ratio
0	458.4	1.6	529.7	2.4	1.4
1	458.5	1.5	529.8	2.3	1.6
5	458.5	1.5	529.8	2.3	1.5
20	458.6	1.5	529.8	2.2	1.6

TABLE 3: XPS Binding Energies/eV of the Pure Sb_2O_3 and FWHM (eV) Depending on the Duration of Milling

milling duration (h)	$Sb3d_{3/2}$	fwhm	O1s	fwhm	$O1s/Sb3d_{3/2}$ ratio
0	539.3	2.0	530.3	2.1	1.3
1	539.4	2.0	530.4	2.1	1.3
5	539.5	2.2	530.3	2.2	1.3
20	539.4	2.1	530.3	2.1	1.4

The binding energies and the width of the signals of the milled TiO_2 did not change either. The observed binding energies were O1s, 529.8 eV; $Ti2p_{3/2}$, 458.4 eV; and $Ti2p_{1/2}$, 464.3 eV (literature values:[19] O1s, 530.0 eV; $Ti2p_{3/2}$, 458.5 eV; and $Ti2p_{1/2}$, 464.2 eV). The signal intensity ratio of O1s and $Ti2p_{3/2}$ of the untreated anatase slightly increased from 1.4. to 1.6 after 20 h milling relative to the untreated sample. The XPS results of the pure oxides are summarized in Tables 2 and 3.

Figure 1 shows the Sb L_3 edge XANES spectra of selected oxidic antimony reference compounds arranged by increasing average oxidation state of the Sb atoms. In all spectra, preedge absorption peaks A at an energy of about 4.135 keV are observed which are attributable to dipole-allowed electronic transitions from the Sb $2p_{3/2}$ orbitals to the (partially) unoccupied Sb 5*s* states. The intensity of these peaks increases on going from Sb(III) to Sb(V) compounds, thus reflecting the progressing depopulation of the 5*s* states with increasing average Sb

oxidation state. It can also be observed that the width of peak A is smallest in the spectrum of $Na[Sb(OH)_6]$, as compared to the peaks of the other Sb(V) compounds $Sb_2O_5 \cdot 3.5\ H_2O$ and $ZnSb_2O_6$. This is due to the isolation of the $[Sb(OH)_6]^-$ ions leading to only a very small dispersion of the 5*s* states in this compound. In the other two Sb(V) compounds investigated, extended covalent bonding occurs and correspondingly the electronic states are broadened. The energy positions of A remain almost unchanged for all reference compounds, irrespective of the changes in oxidation state.

In the energy region above the absorption edge which starts with a second peak B, the spectra show structures that are characteristic for the investigated compounds and can be viewed at as their specific "fingerprints". Whereas B can be attributed to Sb $2p_{3/2} \rightarrow 5d$ transitions and possesses a characteristic shape for all compounds, the structures at higher energies are caused by multiple scattering (MS) processes around the absorbing Sb atoms which strongly depend on the individual environments of the absorbing atoms. To study the effect of local order around the absorbing atoms, it is useful to compare the spectra of crystalline senarmontite and amorphous Sb_2O_3, i.e., compounds with identical chemical composition but different degrees of order. First, it can be stated that the preedge peak A is almost identical in both spectra. This was expected because both compounds contain Sb exclusively in the oxidation state +3 and have similar bonding conditions. In contrast, the structures in the energy region above the edge are quite different: Peak B and additional XANES features observed for senarmontite are broadened and smoothed out in the spectrum of amorphous Sb_2O_3, resulting in a XANES spectrum that is almost featureless except for two broad humps at 4.1525 and 4.1621 keV. Such observations are typical for amorphous compounds and can be explained by a decrease in the short- and medium-range order around the absorbing atoms. An amorphization of crystalline senarmontite can thus clearly be detected in the XANES spectra.

The findings concerning the oxidation states of the samples can be obtained even more clearly by considering the Sb L_1 edge spectra. For the reference compounds, these are shown in Figure 2. The most prominent features are the so-called white lines C at the onset of the edge in the energy region of 4.70 to 4.71 keV. The WLs are caused by $2s \rightarrow 5p$ dipole-allowed transitions of the Sb 2*s* core electrons to the unoccupied $5p_{1/2}$ and $5p_{3/2}$ orbitals which are localized at the absorbing atoms.

At a first glance, a clear distinction between Sb(III) (senarmontite and amorphous Sb_2O_3), mixed-valence Sb(III)/Sb(V) (Sb_2O_4, Sb_6O_{13} and "Sb_2O_5"), and Sb(V) ($Sb_2O_5 \cdot 3.5\ H_2O$, $ZnSb_2O_6$, and $Na[Sb(OH)_6]$) compounds is possible from the line shapes and the energy positions of the white lines. Compounds which contain Sb atoms in only one oxidation state possess spectra which exhibit only one WL at the edge. The energy positions of the WLs of Sb(III) and Sb(V) compounds are clearly separated by 4 to 5 eV and appear at ca. 4.702 to 4.703 keV and at ca. 4.707 keV for Sb(III) and Sb(V) compounds, respectively. This energy shift is mainly caused by the increase of the positive charge on Sb(V) compared to Sb(III), directly increasing the binding energy of the core electrons. On the other hand, the spectra of compounds in which both Sb(III) and Sb(V) are present show split WLs with shapes that can be considered as superpositions of the WLs from single oxidation state Sb(III) and Sb(V) compounds. The maxima of their WL components also appear at ca. 4.703 and 4.707 keV, so that they can be assigned unambiguously to Sb(III) and Sb(V) atoms, respectively. Their respective intensities and the composite line shapes are obviously related to the Sb(III)/Sb(V) ratios in the mixed-valence compounds. Despite these observations, it is not possible to obtain the spectra of the mixed-valence compounds Sb_2O_4 or Sb_6O_{13} by simply superpositioning the spectra of Sb_2O_3 and $Sb_2O_5 \cdot 3.5\ H_2O$ with the ratios 1:1 or 1:2, respectively. This is because the intensities and shapes of the WLs are related not only to the amount of Sb(III) or Sb(V) in the compound but also to the particular chemical environment of these atoms. Nevertheless, an estimation of the Sb(III)/Sb(V) ratio by a qualitative comparison of the WL shapes for chemically similar compounds is possible. For example, comparing the spectra of Sb_6O_{13} and "Sb_2O_5", the Sb(III)/Sb(V) ratio in "Sb_2O_5" can be estimated to be approximately 1:2. This result is in good agreement with a determination of the Sb(III)/Sb(V) ratio in "Sb_2O_5" by Mössbauer spectroscopy.[21]

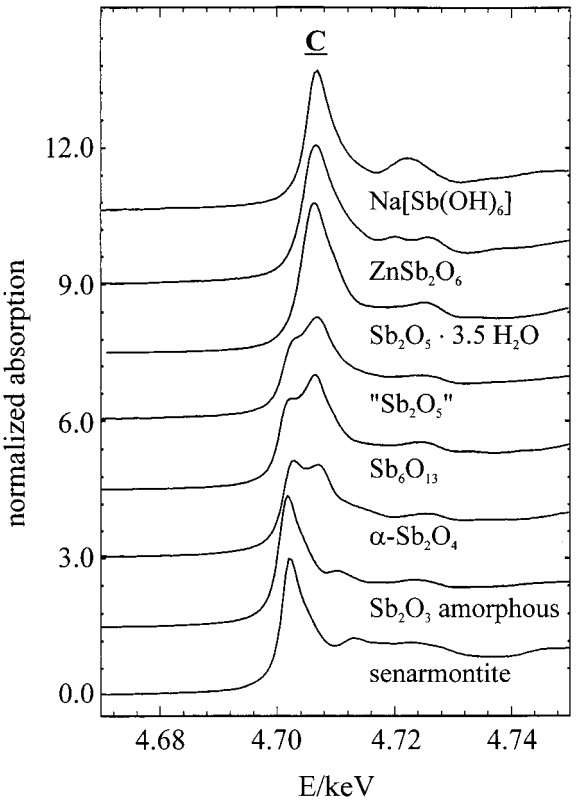

Figure 2. SbL_1 edge XANES spectra of selected oxidic antimony compounds. The spectra are arranged from bottom to top by increasing average oxidation state of the Sb atoms.

Sb_2O_3/TiO_2 Mixtures. In the case of the titania-supported Sb_2O_3, the intensity of the XRD pattern of senarmontite clearly decreased with increasing time of mechanical treatment.

The XP spectrum of a monolayer (ML) Sb_2O_3 on TiO_2 after milling for 1 h clearly showed that the $Sb3d_{3/2}$ signal for the 1ML Sb_2O_3/TiO_2 sample milled for only 1 h has very low intensity as compared to the O1s, Ti2p, or the C1s signal. The latter signal arises from intrinsic graphitic carbon contaminations. It is thus possible to use the C1s peak position for the correction of the energy spectra for steady-state sample charging.[22,23] To obtain reproducibility and internal consistency of binding energies,[24] the Ti2p doublet peak position was also used as binding energy reference. The $Sb3d_{5/2}$ emission of Sb^{3+} is expected at $E_b = 530.0$ eV.[25,26] This signal is completely superimposed by the intense O1s signal. Its estimated value is taken into consideration by the normalization procedure. The O1s contributions from TiO_2 and Sb_2O_3 cannot be resolved because they are almost identical with 530.0 eV[27] and 530.2 eV,[20] respectively.

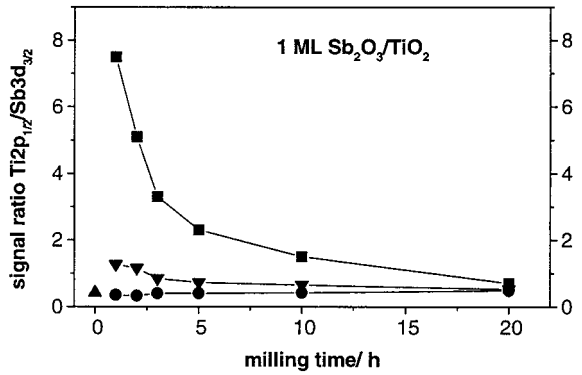

Figure 3. Ti2p/Sb3d XPS intensity ratios of Sb_2O_3/TiO_2 as a function of milling time: ■, Sb_2O_3/TiO_2 after dry milling; ▼, Sb_2O_3/TiO_2 after milling in the presence of 10 wt % H_2O; ●, Sb_2O_3/TiO_2 after dry milling followed by calcination at 673 K for 5 h; ▲, Sb_2O_3/TiO_2 prepared by impregnation from aqueous solution and calcination at 673 K for 5 h.

The intensity of the $Sb3d_{3/2}$ emissions is increasing significantly with the duration of the milling. Only insignificant changes in the binding energies were found from 539.3 eV after 1 h to 539.5 eV after 20 h milling. This indicates that a mechanochemical oxidation of the Sb_2O_3 is not detectable by means of XPS in the case of dry mechanical treatment.

The surface sensitivity of XPS[28] permits the degree of dispersion of a supported species to be detected.[29] In Figure 3 the ratios of the $Ti2p_{1/2}$ and $Sb3d_{3/2}$ signal intensities are plotted versus the time of milling for differently pretreated samples. For the dry milled monolayer system of Sb_2O_3 on TiO_2 it can be clearly seen that the signal ratio decreases with the milling time and therefore the dispersion of Sb oxide increases. This effect is more pronounced at short periods of milling between 1 and 5 h. After 5 h the changes in the signal ratios are smaller and obviously approach a saturation value asymptotically. Therefore, the milling period between 1 and 20 h is well chosen, because still longer mechanical treatments will probably not lead to a higher dispersion of Sb_2O_3.

The decreasing $Ti2p_{1/2}/Sb3d_{3/2}$ intensity ratio qualitatively supports the increasing dispersion of the Sb oxide, but it does not prove or disprove the formation of a true monolayer. The result would be equally consistent with the formation of very tiny clusters as actually suggested by the EXAFS results (see below).

Changing the pretreatment conditions leads to a significant effect on dispersion of Sb oxide. Addition of 10 wt % water to the sample during milling causes an intensification of the $Sb3d_{3/2}$ emission so that the $Ti2p_{1/2}/Sb3d_{3/2}$ ratio reaches values after short milling times (1 h) that are comparable to those observed after 10 to 20 h of dry milling. This effect may be induced by the more pronounced formation of hydroxylated oxo species of the Sb oxide. An analogous effect is well known during thermal spreading of V-oxo species on oxidic supports.[30,31] Also, calcination at 673 K for 5 h after milling for a short period leads to a dispersion as high as that observed for the "wet" milled samples. There is no additional increase of dispersion during calcination for the samples that were milled for longer periods of time. They ultimately reached dispersions of the "dry" milled sample after 20 h, and those for additionally calcined samples or for "wet" milled samples were of the same order of magnitude as the dispersion of conventionally impregnated and calcined samples.

Not only is the dispersion of the Sb oxide affected by a milling and subsequent calcination, but also the oxidation state of the Sb oxide is changing after calcination at 673 K for 5 h.

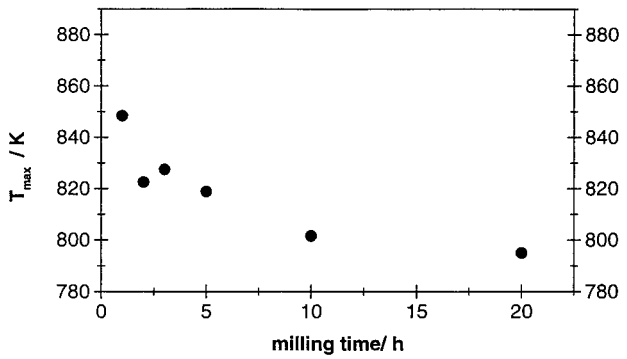

Figure 4. Dependence of the T_{max} values in TPR experiments as a function of milling time.

TABLE 4: XPS Binding Energies and FWHM (eV) of $Sb3d_{3/2}$ and O1s of 1 ML Sb Oxide/TiO_2 Depending on the Duration of Milling and Subsequent Calcination (673 K for 5 h)

milling duration (h)	$Sb3d_{3/2}$	fwhm	O1s	fwhm
1	541.8	2.2	530.1	2.3
5	541.8	2.0	530.1	2.2
20	541.6	2.1	530.0	2.2

The corresponding binding energies for 1 ML Sb_2O_3/TiO_2, depending on duration of milling plus a subsequent calcination at 673 K for 5 h, are summarized in Table 4. This is remarkable because an oxidation of the pure milled Sb_2O_3 did not occur, and the temperature known for the oxidation of the Sb_2O_3 senarmontite (773 K)[26] is 100 °C higher as compared to the present experiments. We conclude therefore that milling induces an important activation step for thermal oxidation because of the mechanical spreading of the oxide or the strong interaction of the supported species with the TiO_2 support. The final product of oxidation is not Sb_2O_4 as one would expect from a bulk phase oxidation.[32] XPS binding energies suggest a Sb(V) oxide with a $Sb3d_{3/2}$ emission at 541.8 eV[20] after 20 h milling as a majority compound on the surface or at least another mixed-valence compound such as Sb_6O_{13}.

TPR yielded a single symmetric signal for the H_2 consumption for the samples of 1ML Sb_2O_3/TiO_2 with the T_{max} depending on the time of mechanical treatment. Figure 4 illustrates the shift of T_{max} from 850 to 795 K for samples after 1 to 20 h of milling. The shape of the TPR signal indicates that the reduction is a one-step process to the final oxidation state. The total H_2 consumption gave three oxidation equivalents of antimony. Starting from Sb^{3+} the reduction product is therefore Sb^0, which was confirmed by XPS after the TPR experiment. We found a binding energy for $Sb3d_{3/2}$ of 537.5 eV, which is in good agreement with the literature value of 537.8 eV.[15] The TPR profiles are illustrated in Figure 5 for samples after 20 h milling without heating, after heating in N_2 for 20 h at 723 K, and after calcination for 20 h at 723 K. It can clearly be seen that heating in a non-oxidizing atmosphere does not influence the reduction behavior (T_{max} at 788−795 K). However, after calcination the T_{max} value shifts to higher temperature, namely 858 K. The profile loses the original symmetry and exhibits a weak shoulder at about 814 K. The shift of T_{max} after calcination is not the result of a redispersion effect as can be concluded from the XPS data. Therefore, the change of reducibility must be an effect due to a different phase of the Sb oxide. The oxidation equivalents calculated from the total amount of H_2 consumed leads to the results summarized in Table 5. It can be concluded from the TPR experiments that the Sb^{3+} oxide is transformed

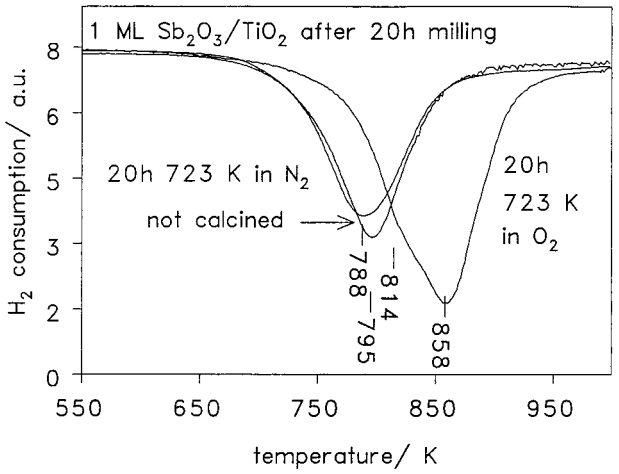

Figure 5. TPR profiles for Sb_2O_3/TiO_2 uncalcined and after calcination for 20 h at 723 K in either N_2 or O_2.

TABLE 5: Changes of the Average Oxidation State of Sb Oxide in the System 1 ML Sb_2O_3/TiO_2 as Calculated from TPR Data in Dependence on the Duration of Milling and Pretreatment

	Sb oxidation states		
milling duration (h)	without pretreatment	20 h 723 K in N_2	20 h 723 K in O_2
1	2.9	3.0	4.7
2	2.9	2.9	4.9
3	3.0	2.9	4.8
5	3.0	2.9	5.1
10	2.9	2.8	5.1
20	3.1	2.9	5.0

into an Sb^{5+} oxidation state after calcination at 673 K. This is in excellent agreement with XPS and XANES results to be discussed next.

Figure 6 shows the Sb L_3 edge XANES spectra of the investigated Sb_2O_3/TiO_2 catalyst precursors, the dry-milled and calcined as well as the wet-milled and calcined ones. The preedge peaks A in the spectra of all uncalcined samples are similar to those of senarmontite and amorphous Sb_2O_3 (Figure 1). This indicates that the oxidation state +3 for the Sb atoms does not change during the milling process, irrespective of the milling time and the H_2O content. In the spectra of the calcined samples, the preedge peaks are more similar to those of α-Sb_2O_4 or Sb_6O_{13}, indicating that during the calcination process Sb(III) is partially oxidized to Sb(V). These results are further confirmed by the analysis of the L_1 edge spectra from which more apparent conclusions concerning the Sb oxidation states can be obtained (see below). A view into the energy region of peak B and the MS region reveals that the features of samples that were milled for only 1 h (both dry or with H_2O) are almost indiscernible from those exhibited by crystalline senarmontite. This shows that the short- to medium-range order around the absorbing Sb atoms is not remarkably altered. Taking the XPS results (Figure 3) into account, which demonstrated significant spreading of Sb_2O_3 across the anatase support after wetmilling for 1 h, it can be concluded that the spreading process occurring at short milling times leaves fragments of the Sb_2O_3 structure unchanged. This can be understood by considering the structure of senarmontite which consists of Sb_4O_6 subunits. Covalent bonding is predominant within these subunits which are held together by weak van der Waals forces. In conclusion, preferentially Sb_4O_6 subunits are dispersed on the support surface after short milling times (e.g. 1 h), and the spreading appears to be more advanced for wet milling as shown by XPS. In contrast,

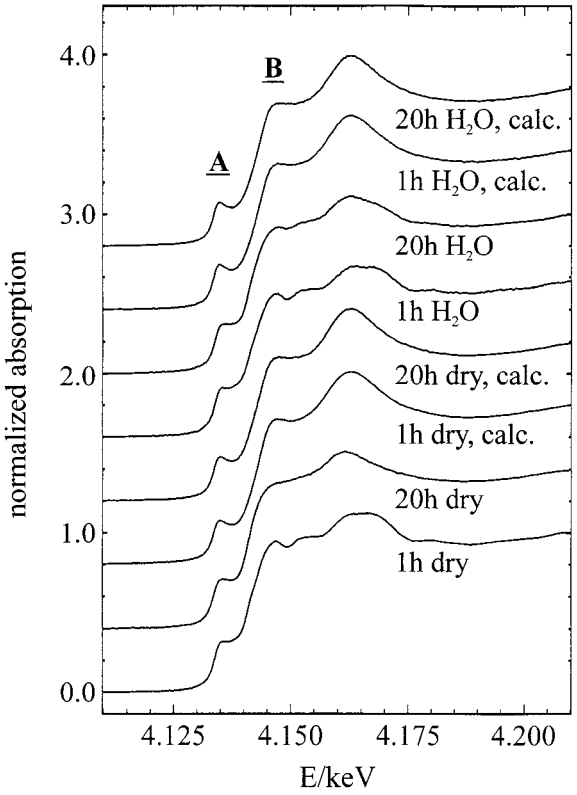

Figure 6. SbL_3 edge XANES spectra of selected oxide catalyst precursors prepared by ball milling of senarmontite with anatase. The type of preparation of the individual samples is indicated in the figure ("calc." means that the samples have been calcined at 673 K for 5 h).

clear differences are apparent between the spectra of dry- and wet-milled samples which were milled for 20 h. In the spectrum of the dry-milled sample, peak B and the other structures are almost completely smoothed out, the only feature present being a hump at 4.1618 keV. In contrast, the spectrum of the sample wet milled for 20 h still largely resembles that of crystalline senarmontite, with only minor smoothing of peak B and of the MS features. These observations lead to the conclusion that dry milling of the samples for 20 h breaks down the Sb_4O_6 subunits, and thus a "real" monolayer distribution may result on the anatase support whereas, in the case of wet milling, Sb_4O_6 units are retained. These suggestions are confirmed by the EXAFS analyses of SbK edge spectra as discussed below. Note, that, although the spectral features have been smoothed out in the spectrum of the dry milled sample, the spectrum differs from that of amorphous Sb_2O_3 (Figure 1), where smoothing also occurs. This difference possibly reflects the presence of atoms from the anatase support in the short- and medium-range coordination around the Sb atoms, which are of course lacking in pure amorphous Sb_2O_3. This observation supports the formation of an Sb oxide monolayer and/or of small SbO_x subunits which are anchored to the TiO_2 support surface.

Calcination of the dry- or wet-milled samples obviously leads to similar materials, nearly independent of the type of previous sample handling and of the calcination time as suggested by the very similar L_3 edge spectra. In addition to the (partial) oxidation evident from the preedge peak A and the L_1 edge spectra (see below), it can be assumed that an amorphization of the Sb oxide and a breakdown of the Sb_4O_6 units has taken place because of the heat treatments.

In Figure 7, the Sb L_1 edge spectra of the catalyst precursors prepared with Sb_2O_3 in the presence or absence of H_2O and by using different milling times are shown. When the samples are

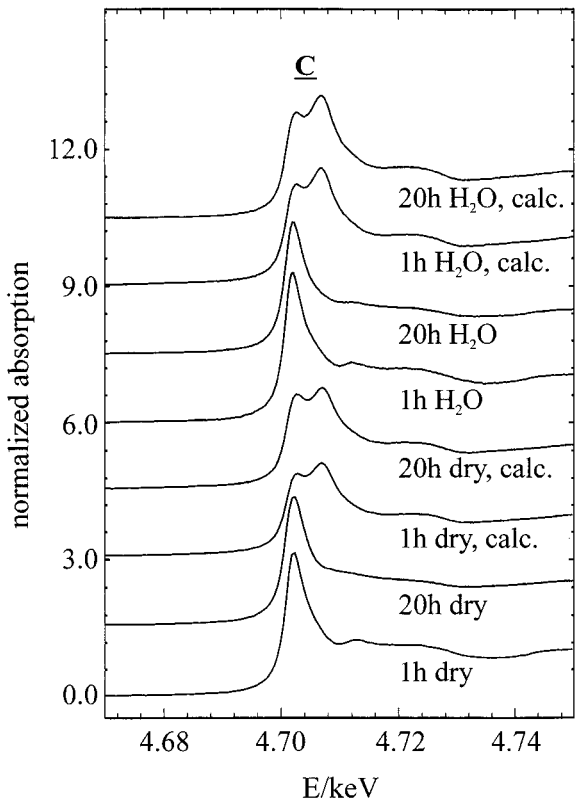

Figure 7. SbL_1 edge XANES spectra of selected oxide catalyst precursors prepared by ball milling of senarmontite with anatase. The type of preparation of the individual samples is indicated in the figure ("calc." means that the samples have been calcined at 673 K for 5 h).

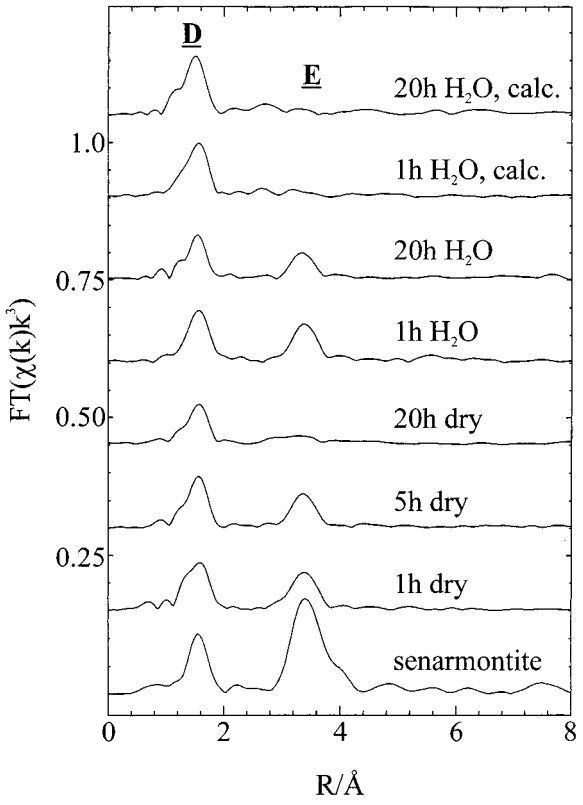

Figure 8. Fourier transforms of the Sb*K* edge EXAFS of Sb_2O_3 (77 K) and of Sb oxide catalyst precursors prepared by ball milling of senarmontite with anatase. The type of preparation of the individual samples is indicated in the figure ("calc." means that the samples have been calcined at 673 K for 5 h).

not calcined, no change of the Sb oxidation states occurs, irrespective of the milling time. This is true for both dry- and wet-milled samples since in all spectra only a single WL C with a maximum at 4.702 keV is present. In the energy region above C, an increased smoothing of the structures is observed with increasing milling time. This effect is stronger in the spectra of the dry-milled samples, similar to the observations at the L_3 edge. Thus, also from Sb L_1 edges an enhanced spreading for dry-milled samples as compared to wet-milled ones is obvious.

The spectra of all calcined samples show a split WL C, substantiating the conclusion that during calcination a non-negligible amount of Sb(III) is oxidized to Sb(V). The shapes of all spectra are very similar, except that for the wet-milled samples the Sb(V) peaks are slightly more pronounced. As mentioned above, the Sb(III)/Sb(V) ratios for the calcined samples can be estimated from the WL shapes. Thus, the antimony oxide part of the samples can be formulated as $Sb_6O_{12+\delta}$ ($0 < \delta < 1$) which makes clear that its average oxidation state is between those of the known crystalline phases Sb_2O_4 and Sb_6O_{13}.

In addition to the Sb *L* edge XANES spectra, we have recorded EXAFS spectra at the Sb *K* edge for those catalyst precursors that are based on Sb_2O_3. The Fourier transforms (FTs) of the EXAFS signals, which represent radial distribution functions around the absorbing Sb atoms, are shown in Figure 8 (no phase shift correction applied). For comparison purposes, the spectrum of pure Sb_2O_3 (measured at 77 K) is also shown. In all spectra, a peak D is observed at ca. 1.7 Å which corresponds to the first coordination shell built up from oxygen atoms. For samples that have been milled for 1 or 5 h, irrespective of the presence or absence of H_2O, this peak does not change significantly except for changes of the shoulder attached to D at lower *R* values. For the samples milled for 20 h, a slight decrease in intensity can be determined for D. It can thus be concluded that the first coordination shell of the Sb(III) atoms remains almost unaltered by milling for 1 to 5 h. Only by an extension of the milling time to 20 h does the order in the first coordination shell begin to decrease. In the FTs of the calcined samples for which only those of the wet-milled samples are shown, D shows only minor changes as compared to uncalcined samples. This indicates that calcination leads to materials with similar order in the first coordination shells around the Sb(III) and Sb(V) atoms, irrespective of the sample treatment before.

Peak E, which is attributable to the second coordination shell built up from Sb atoms, shows a different behavior. This peak is very prominent in pure Sb_2O_3 for which it is caused by three Sb atoms within the Sb_4O_6 unit to which the Sb absorber atom belongs and six additional atoms from neighboring units. In the FTs of samples milled for 1 h (dry or wet), a strong intensity decrease of this peak is detected. This can be explained by the dispersion of Sb_4O_6 units (that are present in senarmontite) on the anatase support surface leading to the loss of order between the Sb_4O_6 units and, hence, to a reduction of the number of contributing second-shell Sb atoms from 9 to 3. In the FTs the intensity of E strongly depends on the sample treatment. For the dry-milled samples, the intensity of E successively decreases with increasing milling time and has vanished almost completely after a milling time of 20 h. In agreement with the XANES results, it can be concluded that not only the medium-range but also the short-range order is affected by the dry milling process, i.e., the molecular Sb_4O_6 units break down and an amorphization down to the second coordination shell takes place. In the case of wet milling, the decrease of the second-nearest neighbor shell E is considerably less pronounced and, even after a milling time

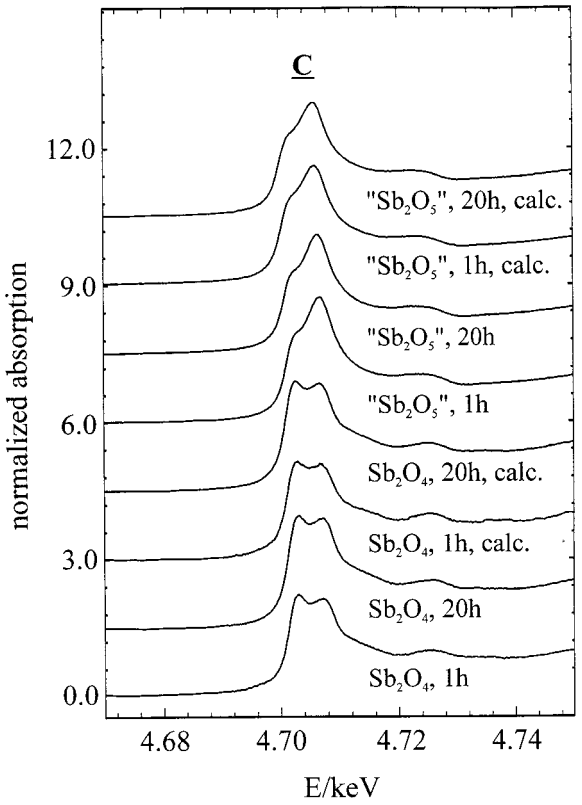

Figure 9. SbL_1 edge XANES spectra of Sb_2O_4/TiO_2 and "Sb_2O_5"/TiO_2 mixtures after various preparation treatments.

of 20 h, E is clearly detectable. This observation confirms the results obtained by the analysis of the Sb *L* edge XANES spectra that the senarmontite medium-range order, i.e., the Sb_4O_6 units, are retained to a high degree in the wet-milled samples, even after long milling times. In the FTs of calcined samples, whether prepared by dry or wet milling, peak E cannot be detected (shown only for wet-milled samples in Figure 8). Thus, independent of the milling time and the presence or absence of water, an amorphization of crystalline Sb_2O_3 and a breakdown of the Sb_4O_6 units occur during the calcination process as also confirmed by the Sb*L* edge spectra.

Sb_2O_4/TiO_2 and "Sb_2O_5"/TiO_2 Mixtures. In addition to the spreading experiments starting with Sb_2O_3, Sb_2O_4 and "Sb_2O_5" were also used as precursors at concentrations corresponding to the monolayer capacity. In contrast to Sb_2O_3/TiO_2 XPS did not give any evidence for surface antimony oxides when Sb_2O_4/TiO_2 was milled and calcined at 723 K for 10 h. Similarly, only extremely weak Sb signals were detectable in the XP spectra after milling "Sb_2O_5"/TiO_2 mixtures followed by calcination at 723 K for 10 h. These results clearly suggest that spreading of Sb oxides does not occur in these systems. These conclusions are supported by TPR experiments which do not show any dependence on milling or calcination. Also, the oxidation states of antimony in these samples remained unchanged during mechanical or thermal treatments.

Supporting evidence for these conclusions was obtained from the Sb L_3 and Sb L_1 edge spectra of samples that have been prepared by dry milling using Sb_2O_4 or "Sb_2O_5" as XANES antimony oxide sources have been recorded (Figure 9). All spectra are identical within experimental and data reduction errors to the spectra of the pure compounds Sb_2O_4 and "Sb_2O_5", respectively, irrespective of milling and calcination times. Thus, it is clear that neither spreading nor changes of the oxidation states occur by milling or calcination. It can thus be concluded that both, Sb_2O_4 and "Sb_2O_5", are not suited for the preparation of antimony oxide catalysts by spreading. A possible explanation for this behavior is that both Sb_2O_4 and "Sb_2O_5" possess three-dimensionally connected structures[21,33] that are not easily transformed into small structural units which can spread over the surface. In contrast, Sb_2O_3 senarmontite is built up from molecular Sb_4O_6 units which can easily be separated from each other. These molecules should easily be able to spread on the anatase support by surface diffusion or transport via the vapor phase.

Conclusions

The addition of antimony oxide to vanadia/titania catalysts is known to enhance the selectivity of these materials for phthalic anhydride production via the oxidation of *o*-xylene.[34,35] On the other hand, little is known about the structure and properties of titania-supported antimony oxides. A physical characterization of the Sb_2O_3/TiO_2 system was therefore carried out in the present work, with materials being prepared by ball milling of the oxide powder mixtures.

The physical techniques applied, namely TPR, XPS, and XAS, provided consistent information on the oxidation state, dispersion, and local environment around Sb atoms of antimony oxide phases and surface species. For comparison purposes we also report the first XANES spectra of well-defined antimony oxide reference compounds.

The Sb L_3 edge XANES spectra show characteristic preedge peaks (peak A) which can be attributed to $2p_{3/2} \rightarrow 5s$ transitions, the intensity of which is related to the Sb oxidation state. In the edge regime, a peak B (assigned as a $2p_{3/2} \rightarrow 5d$ transition) and additional multiple scattering XANES features are indicative fingerprints of the local order around the absorbing Sb atoms. In addition, the position of the $2s \rightarrow 5p$ dipole-allowed white line transitions in Sb L_1 edge spectra (peak C) permit a clear distinction between Sb(III) and Sb(V) compounds.

The major results and conclusions obtained for supported materials are as follows:

1. Milling of the oxide mixtures in the absence of water leads to spreading of Sb_2O_3 across the TiO_2 surface, forming a highly dispersed overlayer. This process is more advanced at shorter milling times in the presence of 10 wt % water. The highest dispersions (comparable to those of materials prepared by impregnation) were obtained after additional calcination at 723 K.

2. During spreading under dry conditions, the typical senarmontite structure is lost and the presence of atoms of the titania support in the vicinity of absorbing Sb atoms is likely. This effect is less pronounced in the presence of water. The first coordination shell of Sb(III) atoms remains almost unaltered by milling up to 5 h in both cases. Only at longer milling times does the order in the first coordination shell begin to be perturbed. Even additional calcination does not significantly affect the order in the first coordination shells. In contrast, the second coordination shell is dramatically perturbed during dry milling, and molecular Sb_4O_6 units present in senarmontite are "cracked" and amorphization down to the second coordination shell takes place. In contrast, the medium-range order is largely retained during milling in the presence of water. Additional calcination leads to an amorphization of crystalline Sb_2O_3 and a "cracking" of the Sb_4O_6 units in the supported overlayer.

3. The milling procedures and the resulting spreading do not induce any oxidation of Sb(III) to higher oxidation states. However, a significant portion of the Sb(III) is oxidized to Sb(V) during addtitional calcination at 673 K. This temperature

is ca. 100 K lower than the known temperature for oxidation of Sb_2O_3.[26] The average oxidation state of the antimony in the antimony oxide overlayer as estimated from XANES spectra would correspond to $Sb_6O_{12+\delta}$ ($0 < \delta < 1$), suggesting that the average oxidation of calcined dispersed antimony oxide supported on titania is between those of the known crystalline phases Sb_2O_4 and Sb_6O_{13}.

Structural characterization and properties of the real ternary catalyst system ($Sb_2O_3 + V_2O_5$) supported on titania will be reported in a forthcoming publication.

Acknowledgment. We thank the Hamburger Synchrotronstrahlungslabor HASYLAB at DESY for allocating beamtime and the HASYLAB staff, especially M. Tischer, L. Tröger, and J. Feldhaus, for kind assistance during the measurements. We are also very grateful to HASYLAB for financial support concerning the travel expenses. Financial support for this work was also provided by the Bayerische Forschungsverbund Katalyse (FORKAT), by the Deutsche Forschungsgemeinschaft (SFB 338), and by the Fonds der Chemischen Industrie. The assistance of Dr. B. Tesche, Max-Planck-Institut für Kohlenforschung, Mülheim, with the electron microscopy studies is gratefully acknowledged. We also thank Prof. Dr. R. K. Grasselli, Universität München, and Dr. H. -J. Eberle, Dr. J. Zühlke, and Dr. P. Storck, Consortium für die elektrochemische Industrie GmbH, München, for their advice and valuable discussions. B.P. acknowledges a PhD scholarship from the Freistaat Bayern.

References and Notes

(1) Albonetti, S.; Cavani, F.; Trifiro, F. *Catal. Rev.* **1996**, *38*, 413.

(2) Weissermel, K.; Arpe, H.-J. *Industrielle Organische Chemie*, VCH: Weinheim, 1994, p 415.

(3) Golunski, S. E.; Jackson, D. *Appl. Catal*. **1989**, *48*, 123.

(4) Andersson, A.; Andersson, S. L. T.; Centi, G.; Grasselli, R. K.; Santani, M.; Trifiro, F. *Proceedings of the 10th International Congress on Catalysis*; Guczi, L., Solymosi, F., Tetenyi, P., Eds.; Akademiai Kiado: Budapest, 1992; A, 691.

(5) Mamedov, E. A.; Corberan, V. C. *Appl. Catal. A* **1995**, *127*, 1.

(6) Thompson, M. R.; Ebner, J. R. In *New Developments in Selective Oxidation by Heterogeneous Catalysis*; Ruiz, P. et al., Eds.; Elsevier Science: Amsterdam, 1992; p 353.

(7) van Hengstum, A. J.; Pranger, J.; van Hengstum-Nijhuis, S. M.; van Ommen, J. G.; Gellings, P. J. *J. Catal*. **1986**, *101*, 323.

(8) Fumagelli, C.; Golinelli, G.; Mazzoni, G.; Messori, M.; Stefani, G.; Trifiro, F. *Catal. Lett*. **1993**, *21*, 19.

(9) Ruiz, P.; Delmon, B. *Catal. Today* **1988**, *3*, 199.

(10) Schild, Ch.; Engweiler, J.; Nickl, J.; Baiker, A.; Hund, M.; Kilo M.; Wokaun, A. *Catal. Lett*. **1994**, *25*, 179.

(11) Heinike, G. *Tribochemistry*; Carl Hanser Verlag: München, 1984.

(12) Zielinski, P. A.; Schulz, R.; Kaliaguine, S.; Van Neste; A. *J. Mater. Res.* **1993**, *8*, 2985.

(13) Zazhiggalov, V. A.; Haber, J.; Stoch, J.; Bogutskaya, L. V.; Bacherikova, J. V. *Proceedings of the 11th International Congress on Catalysis;* Hightower, J. W., Delgass, W. N., Iglesia, E., Bell, A. T., Eds.; Elsevier Science B. V.: Baltimore, 1996; Vol. 101 B, p 1039.

(14) Horowitz, H. S.; Blackstone, C. M.; Sleight, A. W.; Teufel, G. *Appl. Catal*. **1988**, *38*, 193.

(15) Bianconi, A. In *X-ray Absorption* (Chemical Analysis Vol. 92); Koningsberger, D., Prins, R., Eds.; Wiley: New York, 1988.

(16) Chaboy, J.; Benfatto, M.; Davoli, I. *Phys. Rev. B*, **1995**, *52*, 10014.

(17) Roozeboom, F.; Fransen, T.; Mars, P.; Gellings, P. J. *Z. Anorg. Chem.* **1979**, *49*, 25.

(18) Dwyer, D. J.; Cameron, S. D.; Gland, J. *Surf. Sci*. **1985**, *159*, 430.

(19) Ressler, T. *J. Phys. IV France*, **1997**, *7*, C2−269.

(20) Izquierdo, R.; Sacher, E.; Yelon, A. *Appl. Surf. Sci*. **1989**, *40*, 175.

(21) Steward, D. J.; Knop, O.; Ayasse, C.; Woodhams, F. W. D. *Can. J. Chem.* **1972**, *50*, 690.

(22) Swift, P. *Surf. Interface Anal.* **1982**, *4*, 47.

(23) Defossé, C. In *Chemical Industries/15*; Delannay, F., Ed.; Marcel Dekker: New York, Basel, 1984, p 225.

(24) Brundle, C. R. *Appl. Spectrosc.* **1971**, *8*, 25.

(25) Wagner, C. D. *Discuss. Faraday Soc.* **1975**, *60*, 291.

(26) Morgan, W. E.; van Wazer, J. R.; Stec, W. J. *J. Am. Chem. Soc.* **1973**, *95*, 953.

(27) Wang, L.-Q.; Baer, D. R.; Engelhard, M. H. *Surf. Sci.* **1994**, *320*, 295.

(28) Ertl, G.; Küppers, J. *Low Energy Electrons and Surface Chemistry*; VCH: Weinheim, 1985, p 55.

(29) Niemandsverdriet, J. W. *Spectroscopy in Catalysis*; VCH: Weinheim, 1993, p 51.

(30) Hausinger, G.; Schmelz, H.; Knözinger, H. *Appl. Catal.* 1988, *39*, 267.

(31) Shan, S.; Hönicke, D. *Chem. Eng. Technol.* **1989**, *61*, 321.

(32) Centers, P. W. *J. Sol. Chem.* **1988**, *72*, 303.

(33) Amador, J.; Gutiérrez Puebla, E.; Monge, M. A.; Rasines, I.; Ruíz Valero, C. *Inorg. Chem.* **1988**, *27*, 1367.

(34) German patent DE 3045624C2; European patent EP 522871A1.

(35) Wainwright, M. S.; Hoffmann, T. W. *Can. J. Chem. Eng*. **1977**, *55*, 557.